IEEE Access
Multidisciplinary | Rapid Review | Open Access Journal

Received November 27, 2020, accepted December 21, 2020, date of publication December 28, 2020,
date of current version January 6, 2021.

Digital Object Identifier 10.1109/ACCESS.2020.3047650

Dynamic Modeling and Error Analysis of a Cable-Linkage Serial-Parallel Palletizing Robot

HUIHUI SUN[1,2], YUJIE ZHANG[1,2], BIN XIE[3], AND BIN ZI[3]
[1]College of Mechanical and Electrical Engineering, North China Institute of Science and Technology, Langfang 065201, China
[2]Laboratory of Safety Monitoring of Mining Equipment, Langfang 065201, China
[3]School of Mechanical Engineering, Hefei University of Technology, Hefei 230009, China

Corresponding author: Yujie Zhang (zhangyujiebetter@163.com)

This work was supported in part by the Fundamental Research Funds for the Central Universities under Grant 3142019055, in part by the National Natural Science Foundation of China under Grant 51925502, and in part by the Langfang Science and Technology Research and Development Plan under Grant 2018011007 and Grant 2019011058.

ABSTRACT The efficiency and accuracy for parallel robot play a significant role in the industrial production process. In order to further improve the motion performance of parallel robot, this paper focuses on the study of mechanism design, dynamic modeling and error analysis of a cable-linkage serial-parallel palletizing robot (CSPR). Firstly, the CSPR is designed as a series-parallel hybrid mechanism driven by flexible cables, which can effectively reduce the inertia and improve the dynamic response. As is known that kinematic design optimization of compliant mechanisms requires accurate yet efficient mathematical models, the kinematics and dynamic models are established by the homogeneous coordinate transformation method and Lagrange equation. Based on the dynamic mathematical model of the robot, a variety of sensors are chosen to construct the hardware control system and the sliding mode variable structure control strategy is also designed based on motion errors. Then, the motion performance and load carrying capacity of the CSPR were analyzed and compared in different operating conditions respectively, and the results verify the validity and efficiency of the mechanism.

INDEX TERMS Series-parallel mechanism, dynamic modeling, motion performance, error analysis.

I. INTRODUCTION

Palletizing operation is an important and fundamental task for production [1]. Meanwhile, that is also one of the most monotonous and heavy laborious works in the factory. Fortunately, palletizing robots can accurately and efficiently take the place of humankind to handle changing palletizing tasks [2]. Palletizing robots which have three basic categories including serial, parallel, and hybrid robots have attracted continuous interests in the field of robotics [3]. Introduced in the 1980s, the palletizing robots are developed to implement the grabbing, handling, stacking, and unstacking tasks. Currently, employment of palletizing robots in manufacturing has been a value-added entity for the company in gaining their competitive advantages [4]. Therefore, it is necessary to change the mechanism, optimize the control algorithm and improve the motion performance of the palletizing robots [5], [6].

The conventional palletizing robot is a series or parallel structure composed of rigid link body, such as Multi-joint manipulator and delta robot [7]. Multi-joint manipulator is the representative of serial palletizing robot, which has the characteristics of simple structure, convenient control system and low cost [8]. However, because each joint is independent, accumulated errors will occur in the process of motion, resulting in low positioning accuracy [9]. The delta robot is a typical spatial three DOF parallel mechanism,which has the advantages of large stiffness, high repeat positioning accuracy and good dynamic performance. However, its workspace is confined to a small area [10]. In addition, both of the kinds robots have a disadvantages that cannot be ignored. That is, the high inertia of multiple rigid links and actuators on the joints greatly limits the further improvement of the palletizing performance [11].

In order to solve this problem of the high inertia, the cable parallel manipulators (CPMs) have been studied by many researchers and employed in various applications including palletizing [12]. The CPMs have a parallel configuration with higher stiffness, lower inertia, and larger workspace than traditional mechanisms [13]. These characteristics have attracted wide interest in the past few decades, which have been used for construction, leg exoskeleton, material manipulation and astronomical observation. However, due to the fact that the cables can only provide positive tensions and

The associate editor coordinating the review of this manuscript and approving it for publication was Hassen Ouakad.

the cable interferences and collisions always lead to unpredictable behavior [14], many complicated actions in palletizing are difficult to complete by CPMs. To resolve this issue, the CSPR combines the advantages of series-parallel mechanism and CPMs, and replace the rigid rods by multiple flexible cables. Then, the servo motors and reducers with great weight are placed on a platform, which can effectively reduce the motion inertia, expand workspace [15], [16].

As is known that kinematic design optimization of compliant mechanisms requires accurate yet efficient mathematical models [17]. The kinematics is to study the motion characteristics of each joint and the end-effector. It mainly studies the higher-order derivatives of position variables with respect to time [18]. For serial robots, the forward kinematics solution is much less difficult than the inverse kinematics. But for parallel robots, the results are just the opposite [19]. At present, the methods for solving the positive and inverse kinematics of the series and parallel mechanisms mainly include analytical method and numerical optimization method. Analytical method is to use algebraic or geometric methods to solve the solution directly, and obtain a unitary multiple equation by elimination. However, with the increase of the number of DOF of the mechanism, the difficulty of obtaining an analytical solution will also increase, and especially for redundant manipulator, it is particularly difficult to choose an appropriate solution from the answers. The Numerical optimization method is to transform kinematics issue into an numerical optimization issue. For example, the Jacobian matrix inversion method, using the instantaneous kinematics to approximate the results infinitely with the idea of ''differentiation'', is a typical application. In this paper, the Denavit-Hartenberg (D-H) homogeneous transformation matrix method is be used to Kinematic modeling for the CSPR, and the spatial position and attitude relationship of end-effector and joints are described by a 4×4 square matrix, thus the kinematics equation of the CSPR can be further obtained.

The CSPR is a coupled multi-body system with serious nonlinearity [20], [21]. Dynamics research can optimize the structure design, modify the motion control process and improve the real-time control performance [22]. The primary task of dynamic analysis is to establish its model accurately. Because of the flexibility and nonlinearity of the cables, the dynamic model of cable-driven mechanism will be very complex. At present, the common dynamic modeling methods main include Lagrange method, Newton-Euler method, Gauss method, Kane method and virtual work method [23]. Lagrange method is more widely used in solving dynamics issues, and the Lagrange dynamic equation is established based on the kinetic and potential energy of the system, which has explicit structure and clearly physical meaning [24]. The derivation process is relatively simple, and the concise form is convenient for understanding the dynamic characteristics of the CSPR. After dynamic modeling, dynamic simulation will always be used to verify the reliability of the model. The motion process is controlled by a complex torque functions generated by the joint actuator. The functions is determined by the controller. A controller for the palletizing robot not only affects the dynamic characteristics, but also has a great impact on the production efficiency, product cost and production safety.

Objectively speaking, establishing a closed-loop control system supported by a variety of sensors to reduce motion errors and jitter is of great significance for the CSPR. In the system, the sensors are an essential part. The internal sensors are used to obtain its own motion information, and the external sensors are to obtain environmental information. Then, the acquired information are fed back to the controller for real-time compensation of motion errors through intelligent control algorithms [25]. During the development of the control system, many excellent control algorithms have been applied in the series-parallel mechanism, such as traditional PID control, fuzzy control, neural network control, variable structure control robust control and so on. He, W *et al.* [26] proposed an adaptive neural network (NN) control for the robotic system with full-state constraints, and the adaptive NNs are adopted to handle system uncertainties and disturbances to prevent the violation of the full-state constraints. Roy, S *et al.* [27] presented an adaptive time-delayed sliding mode control for trajectory tracking control of a class of uncertain Euler-Lagrange systems, which uses artificial time delay to approximate the unknown dynamics through time-delayed logic, and the switching logic provides robustness against the approximation error. Guan, JS *et al.* [28] sutdyed a robust adaptive Takagi-Sugeuo-Kang fuzzy cerebellar model articulation controller (RATFC) and applied it to a robot manipulator to achieve high-precision position and speed control. A Takagi-Sugeuo-Kang fuzzy cerebellar model articulation controller is adopted, and the parameters are regulated by the derived adaptable rules, which has mitigated approximation-based errors. Xu, JM *et al.* [29] presents an adaptive sliding mode control method for nonlinear systems. L.Angel *et al.* [30] presents the tracking control for a robotic manipulator type delta employing fractional order PID controllers with computed torque control strategy. The CSPR, as a combination of series-parallel and cable-linkage driven mechanisms, is a strong nonlinearity, time-varying system, the control process is much more complex [31]. The system framework and control principles with multi-sensors for the CSPR will be built to make a foundation for the experimental prototype.

The rest of the paper is arranged as follows. In section 2, the mechanical design of the CSPR is described in detail, and the DOF of the CSPR is calculated to determine the number of the driven-cable; Section 3 establishes kinematic and dynamic model of the CSPR based on homogeneous coordinate transformation method and Lagrange equation. Motion control system with multi-sensors designed for the CSPR is provided in Section 4. Section 5 presents the simulation results about motion errors and to verify the feasibility of the mechanism and the reliability of the model. The conclusions of this paper are drawn in Section 6.

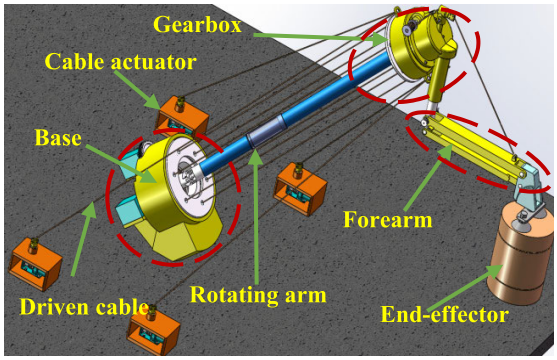

FIGURE 1. The simplified 3-D model of the CSPR.

TABLE 1. Parameters of dof for the CSPR.

	CSPR	Conventional manipulator
Body weight	30kg	100-200kg
Carrying capacity	100kg	5-30kg
maximum range	1750mm	1000-2000mm
Position accuracy	0.5mm	0.02-2mm
Max velocity	800mm/s	300-1500mm/s

II. MECHANICAL DESIGN

A. MECHANICAL STRUCTURE

The CSPR is a cable-linkage series-parallel hybrid-driven palletizing robot with six degrees. This structure is designed to reduce the working inertia and expand the working space of without reducing the carrying capacity. Therefore, the driven-cables are adopted to replace the driving motor of the joints so as to improve the rapid response of the robot.

As shown in Figure 1, the CSPR is composed of the base, rotating arm, forearm, gearbox, driven-cable and end-effector. To improve the working space, the rotating arm is mounted at an acute angle with the horizontal plane, and it consists of a driving rod and six cables with the same length. The six cables can ensure the Base and the gearbox keeping parallel, and the driving rod transmits torque to the gearbox. There are four main driven-cable used to drive rotating arm, and one ancillary driven-cable is used to drive the forearm. All the cable-actuators are placed on the ground to reduce the weight of the manipulator.

In order to reflect the characteristics of CSPR, the performance parameters of the robot are compared with the conventional series robot, and the result shown as Table 1. From Table 1, it can be get that the CSPR has lighter body mass, greater load capacity, greater working speed and workspace, but the repositioning accuracy need to be further enhanced.

B. DEGREE OF FREEDOM CALIBRATION

The mechanism diagram of the CSPR is shown in Figure 2.

In a robot system, the number of drivers must be more than or equal to the *DOF*. The *DOF* of the CSPR needs to be calibrated, and the number of driven-cables must satisfy the formula: $n \geq M+1$, which is at least one more than the *DOF*.

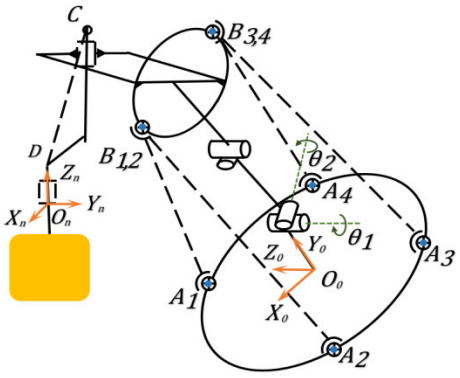

FIGURE 2. Mechanism diagram of the CSPR.

TABLE 2. Parameters of dof for the CSPR.

Parameter	*d*	*n*	*g*	*v*	*M*
Value	*5*	*12*	*13*	*0*	*3*

According to the calculation method of closed redundant mechanism proposed in literature [32], [33], the degrees of freedom of the robot can be expressed as:

$$M = d\,(n-g-1) + \sum f_i + v \tag{1}$$

where, $d = 6-\lambda, \lambda$ is the common constraint of the mechanism.; n is number of components; g is the number of motion pairs; f_i is the degree of freedom of the ith motion pair; v is number of closed redundant constraints. According to the characteristics of the mechanism, the values of parameters in *Eq.*(1) are shown in Table 2.

According to Table 2, the degree of freedom of the CSPR is three, so it is correct and necessary for the CSPR to use four driven-cable to drive rotating arm.

III. KINEMATIC AND DYNAMIC ANALYSIS

A. KINEMATIC MODELING

After analyzing the motion characteristics of the CSPR, *Z-Y-X* Euler Angle is adopted to describe the reference coordinate based on Homogeneous coordinate transformation method. The reference coordinate system diagram of the CSPR is shown in Figure 3.

The $O_0-X_0Y_0Z_0$ is global coordinateis located at the Base of CSPR, and the local coordinate system $O_n-X_nY_nZ_n$ is located at each joint. Assuming that ${}^m_nT$ denotes transformation matrix of Cartesian $O_n-X_nY_nZ_n$ with reference to Cartesian $O_m-X_mY_mZ_m$, orientation and position of end-effector can be expressed as:

$${}^0_6T = {}^0_1T\,{}^1_2T\,{}^2_3T\,{}^3_4T\,{}^4_5T\,{}^5_6T \tag{2}$$

where:

$$\begin{cases} {}^0_1T = \begin{bmatrix} {}^0_1R & \Delta_1 \\ \vec{0} & 1 \end{bmatrix}; {}^1_2T = \begin{bmatrix} {}^1_2R & \Delta_2 \\ \vec{0} & 1 \end{bmatrix}; {}^2_3T = \begin{bmatrix} {}^2_3R & \Delta_3 \\ \vec{0} & 1 \end{bmatrix} \\ {}^3_4T = \begin{bmatrix} {}^3_4R & \Delta_4 \\ \vec{0} & 1 \end{bmatrix}; {}^4_5T = \begin{bmatrix} {}^4_5R & \Delta_5 \\ \vec{0} & 1 \end{bmatrix}; {}^5_6T = \begin{bmatrix} {}^5_6R & \Delta_6 \\ \vec{0} & 1 \end{bmatrix} \end{cases}$$

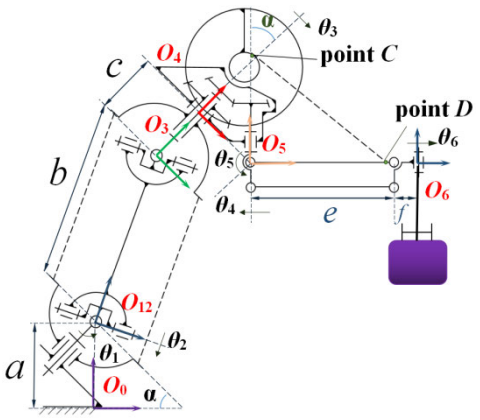

FIGURE 3. Reference coordinate system diagram of the CSPR.

Δ in transformation matrix ${}^{m}_{n}T$ is the length vector of each joint:

$$\begin{cases} \Delta_1 = [0\ a0]^T;\ \Delta_2 = [0\ b0]^T \\ \Delta_3 = [0\ c0]^T;\ \Delta_4 = [0\ d0]^T \\ \Delta_5 = [e\cos\theta_5 + fe\sin\theta_5 0]^T \\ \Delta_6 = [0\ a0]^T \end{cases} \tag{3}$$

As shown in Figure 3, ${}^{m}_{n}R$ in transformation matrix can be described by Euler angle based on angle parameters:

$$\begin{aligned} {}^{m}_{n}R_{Z'Y'X'} &= R_Z(\alpha)R_Y(\beta)R_X(\gamma) \\ &= \begin{bmatrix} c\alpha & -s\alpha & 0 \\ s\alpha & c\alpha & 0 \\ 0 & 0 & 1 \end{bmatrix} \begin{bmatrix} c\beta & 0 & s\beta \\ 0 & 1 & 0 \\ -s\beta & 0 & c\beta \end{bmatrix} \begin{bmatrix} 1 & 0 & 0 \\ 0 & c\gamma & -s\gamma \\ 0 & s\gamma & c\gamma \end{bmatrix} \end{aligned} \tag{4}$$

where, $+c$ is represent as "cos", s is represent as "sin". α, β, γ are Euler angles of every joint.

Eq.(5) can also be simplified to:

$${}^{m}_{n}R = \begin{bmatrix} c\alpha c\beta & c\alpha s\beta s\gamma - s\alpha c\gamma & c\alpha s\beta c\gamma + s\alpha s\gamma \\ s\alpha c\beta & s\alpha s\beta s\gamma + c\alpha c\gamma & s\alpha s\beta c\gamma - c\alpha s\gamma \\ -s\beta & c\beta s\gamma & c\beta c\gamma \end{bmatrix} \tag{5}$$

By combining Eqs.(2)∼(5), it can be obtained that:

$${}^{0}_{6}T = \begin{bmatrix} r_{11} & 0 & r_{13} & p_1 \\ 0 & 1 & 0 & p_2 \\ r_{31} & 0 & r_{33} & p_3 \\ 0 & 0 & 0 & 1 \end{bmatrix} \tag{6}$$

where

$$\begin{cases} r_{11} = r_{33} = \cos(\theta_4 + \theta_6);\ r_{13} = -r_{31} = \sin(\theta_4 + \theta_6) \\ p_1 = k_3 - k_1\cos\theta_2\sin(\theta_1 - \pi/4) + (k_2\cos\theta_5 + 0.1)\cos\theta_4 \\ p_2 = k_2\sin\theta_5 + k_1\cos\theta_2\sin(\theta_1 + \pi/4) - k_4 \\ p_3 = k_1\sin\theta_2 - 0.1\sin\theta_4 - k_2\cos\theta_5\sin\theta_4 \end{cases}$$

Eq.(6) represents the total transformation of coordinates between the end-effector and the Base, and the six joint rotation angle variables of the CSPR are $\theta_1, \theta_2, \theta_3, \theta_4, \theta_5, \theta_6$.

Further, the driving mechanism of CSPR is the 5 driven-cables. As shown in Figure 2, the four driven-cable of Rotatory-arms can are $B_iA_i(i = 1, 2, 3, 4)$, and the driven-cable of forearm is defined as DC. Based on Eq,(2)∼(5), the length of each driven-cable can be calculated by Eq(7):

$$\begin{cases} l_{B_iA_i} = [({}^{0}\ell_{Ai} - {}^{0}_{4}T \cdot {}^{4}\ell_{Bi})({}^{0}\ell_{Ai} - {}^{0}_{4}T \cdot {}^{4}\ell_{Bi})^T]^{1/2} \\ l_{DC} = [({}^{4}\ell_{C} - {}^{4}_{5}T \cdot {}^{5}\ell_{D})({}^{4}\ell_{C} - {}^{4}_{5}T \cdot {}^{5}\ell_{D})^T]^{1/2} \end{cases} \tag{7}$$

where, ${}^{0}\ell_{Ai} = (x_{Ai}, 0, z_{Ai}, 1)$, ${}^{4}\ell_{Bi} = (x_{Bi}, 0, z_{Bi}, 1)$, $l_{B_iA_i}$ is the length of the ith cable. l_{DC} is the length of driven-cable of forearm.

B. DYNAMIC MODELING

The CSPR is a seriously nonlinear coupled multi-body system. The dynamic model is the theoretical basis of motion control. In this section, Lagrange method will be used to analyze the dynamics of the robot. According to the kinematics analysis of the CSPR, the DOF of the end-effector include three translational DOF, $({}^{0}x_6, {}^{0}y_6, {}^{0}z_6)$ and three rotational DOF $({}^{0}\theta_x, {}^{0}\theta_y, {}^{0}\theta_z)$, respectively. The Jacobian matrix is a 6×6 square matrix. According to *Eq.*(6), the functions of end-effector position and joint variables are:

$$\begin{cases} {}^{0}x_6 = f_1(\theta_1, \cdots, \theta_6)\ {}^{0}y_6 = f_2(\theta_1, \cdots, \theta_6) \\ {}^{0}z_6 = f_3(\theta_1, \cdots, \theta_6) \\ {}^{0}\theta_x = f_4(\theta_1, \cdots, \theta_6)\ {}^{0}\theta_y = f_5(\theta_1, \cdots, \theta_6) \\ {}^{0}\theta_z = f_6(\theta_1, \cdots, \theta_6) \end{cases} \tag{8}$$

Then derive the multivariate function and calculate the differential function of each joint variable

$$\begin{cases} \delta\left({}^{0}x_6\,{}^{0}y_6\,{}^{0}z_6\right) = \dfrac{\partial f_i}{\partial\theta_1}\delta\theta_1 + \cdots + \dfrac{\partial f_i}{\partial\theta_6}\delta\theta_6 \quad (i = 1, 2, 3) \\ \delta\left({}^{0}\theta_x\,{}^{0}\theta_y\,{}^{0}\theta_z\right) = \dfrac{\partial f_i}{\partial\theta_1}\delta\theta_1 + \cdots + \dfrac{\partial f_i}{\partial\theta_6}\delta\theta_6 \quad (i = 4, 5, 6) \end{cases} \tag{9}$$

then, *Eq.*(9) can also be simplified to vector expression:

$$\delta^{0}\varsigma = \frac{\partial^{0}F}{\partial\Theta}\delta\Theta \tag{10}$$

where, $\varsigma = \left[x_6, y_6, z_6, \theta_x, \theta_y, \theta_z\right]$ $\Theta = [\theta_1, \theta_2, \theta_3, \theta_4, \theta_5, \theta_6]$, $F = [f_1, f_2, f_3, f_4, f_5, f_6]$

Therefore. the 6×6 partial derivative matrix ${}^{\partial^{0}F}/_{\partial\Theta}$ in *Eq.*(10) is the Jacobian matrix $J(\Theta)$ of the CSPR. Therefore, it can be rewritten as:

$$\delta^{0}\varsigma = J(\Theta)\delta\Theta, \quad \dot{\varsigma} = J(\Theta)\dot{\Theta} \tag{11}$$

In order to obtain the driving force and torque of the joints, the Lagrange dynamic equation of the CSPR will be established in the next based on Jacobian matrix. Lagrange function is defined as the difference between kinetic energy and potential energy of the CSPR system, that is:

$$L = E - U = \sum_{i=1}^{5}\left(\frac{1}{2}m_iv_i^2 + \frac{1}{2}j_i\omega_i^2\right) - \sum_{j=1}^{5}(m_jgh_{zj} - U_{j0}) \tag{12}$$

where, U_{j0} represents the initial potential energy of each moving part, and hz_j represents the centroid displacement of each moving part in the Z direction.

According to the Lagrange function, the generalized driving force and torque of end-effector motion can be expressed as:

$$\begin{aligned}
&F_x = \frac{d}{dt}\left(\frac{\partial L}{\partial {}^0\dot{x}_6}\right) - \frac{\partial L}{\partial {}^0x_6}; F_y = \frac{d}{dt}\left(\frac{\partial L}{\partial {}^0\dot{y}_6}\right) - \frac{\partial L}{\partial {}^0y_6};\\
&F_z = \frac{d}{dt}\left(\frac{\partial L}{\partial {}^0\dot{z}_6}\right) - \frac{\partial L}{\partial {}^0z_6}\\
&T_x = \frac{d}{dt}\left(\frac{\partial L}{\partial {}^0_6\dot{\theta}_x}\right) - \frac{\partial L}{\partial {}^0_6\theta_x}; T_y = \frac{d}{dt}\left(\frac{\partial L}{\partial {}^0_6\dot{\theta}_y}\right) - \frac{\partial L}{\partial {}^0_6\theta_y};\\
&T_z = \frac{d}{dt}\left(\frac{\partial L}{\partial {}^0_6\dot{\theta}_z}\right) - \frac{\partial L}{\partial {}^0_6\theta_z}
\end{aligned} \tag{13}$$

So the vector of generalized force system acting on the end-effector is:

$$T_\tau = \begin{bmatrix} F_x & F_y & F_z & T_x & T_y & T_z \end{bmatrix}^T \tag{14}$$

Similarly, the vector of torque acting on each joint can be expressed as:

$$\tau = [M_1\ M_2\ M_3\ M_4\ M_5\ M_6]^T \tag{15}$$

The virtual angular displacement of each joint is $\delta_\theta = [\delta_{\theta 1}\delta_{\theta 2}\delta_{\theta 3}\delta_{\theta 4}\delta_{\theta 5}\delta_{\theta 6}]^T$, The virtual displacement of the end-effector is: $\delta_k = [\delta_{k1}\delta_{k2}\delta_{k3}\delta_{k4}\delta_{k5}\delta_{k6}]^T$, the virtual work done by the driving torque of each joint variable and done by the generalized force system on the end-effector can be calculated:

$$\begin{cases}
W_\tau = \tau^T\delta_\theta = M_1\delta_{\theta 1} + M_2\delta_{\theta 2} + M_3\delta_{\theta 3} + M_4\delta_{\theta 4}\\
\qquad +M_5\delta_{\theta 5} + M_6\delta_{\theta 6}\\
W_T = T_\tau^T\delta_k = F_x\delta_{k1} + F_y\delta_{k2} + F_z\delta_{k3} + T_x\delta_{k4}\\
\qquad +T_y\delta_{k5} + T_z\delta_{k6}
\end{cases} \tag{16}$$

According to the principle of energy conservation and principle of virtual work, W_τ represents the total virtual work done by the joints and cables, and W_T represents the virtual work done by the generalized force system on the end-effector [34], [35]. Based on the law of energy conservation, the virtual work done through the virtual displacement are equal, so it can be get *Eq.*(17) according to *Eq.*(16):

$$T_\tau^T\delta_k = \tau^T\delta_\theta \tag{17}$$

where, T_τ is the vector of generalized force system acting on the end-effector, δ_k is virtual displacement; τ the vector of torque acting on each joint, and δ_θ is the virtual angular displacement.

According to the kinematic equation in *Eq.* (11), the relationship between the virtual angular displacement δ_θ and virtual displacement δ_k of the end-effector can be expressed as:

$$\delta_k = {}^0J\,(\Theta)^T\delta_\theta \tag{18}$$

Substituting *Eq.* (17) into *Eq.*(18) can be obtained as:

$$\tau = {}^0J\,(\Theta)^T T_\tau \tag{19}$$

During the entire operation process, the cables remain tensed, which provide the driving force for the manipulator. Similarly, according to the Lagrange equation shown in Eq.(12), the tension for every cable can be as:

$$\begin{aligned}
&S_1 = \frac{d}{dt}\left(\frac{\partial L}{\partial \dot{l}_1}\right) - \frac{\partial L}{\partial l_1}; \quad S_2 = \frac{d}{dt}\left(\frac{\partial L}{\partial \dot{l}_2}\right) - \frac{\partial L}{\partial l_2};\\
&S_3 = \frac{d}{dt}\left(\frac{\partial L}{\partial \dot{l}_3}\right) - \frac{\partial L}{\partial l_{36}}; \quad S_4 = \frac{d}{dt}\left(\frac{\partial L}{\partial \dot{l}_4}\right) - \frac{\partial L}{\partial l_4};
\end{aligned} \tag{20}$$

where, $S_{1,}S_{2,}S_3S_4$ the represent tensions of the cables and $l_1, l_2, l_{3,}l_4$ are the length of the cables.

Finally, according to the kinematic relationship between the end effector and each joint, the driving torque of each joint and the traction force of each driven-cable can be calculated.

IV. CONTROL STRATEGY

Compared with the traditional series equipment, the weight and inertia of the hybrid palletizing robot are significantly reduced. In order to further improve the motion performance of the robot and ensure the safety and reliability, it is necessary to is design a closed loop control system with fast response and strong information processing ability. This system consists of industrial computer, motion control board, servo motor and human-computer interaction interface. A variety of sensors are used to measure the position and orientation of the CSPR to ensure its safety operation. As shown in Figure 4, the cables are the main driving part of the parallel robot, and the driving force and length are the most important parameters that need to be measured. So the displacement sensors and tension sensors are installed on the five driven-cables. Servo motor with rotary encoder is also used to obtain angular displacement and angular velocity of cable actuator. The rotating arm is the driving mechanism of the forearm, and the rotation angle of the rotating arm must be measured by the angular displacement sensor. At the same time, the angular displacement sensors are also set on every joint to collect the value of the angular displacement. In order to ensure the accurate positioning and safety operation of the palletizing robot, the infrared sensors and ultrasonic sensors are essential to avoid obstacles in real time. The attitude and acceleration parameters of end-effector are the most important indexes to the stability palletizing, so the attitude and acceleration sensors are set on the end-effector to constitute a closed-loop control system.

The main performance parameters of the sensors are listed in Table 3.

As shown in Figure 5, the software of the control system includes: initialization program of DSP, detection subroutine, ADC interrupt service subroutine, regulation control procedure, driver control procedure, network communication procedure and so on. In order to improve the motion precision of CSPR, a sliding mode control strategy is designed based on motion error. The tracking angular displacement error is defined as:

$$e = \theta_{ai} - \theta_{qi} \tag{21}$$

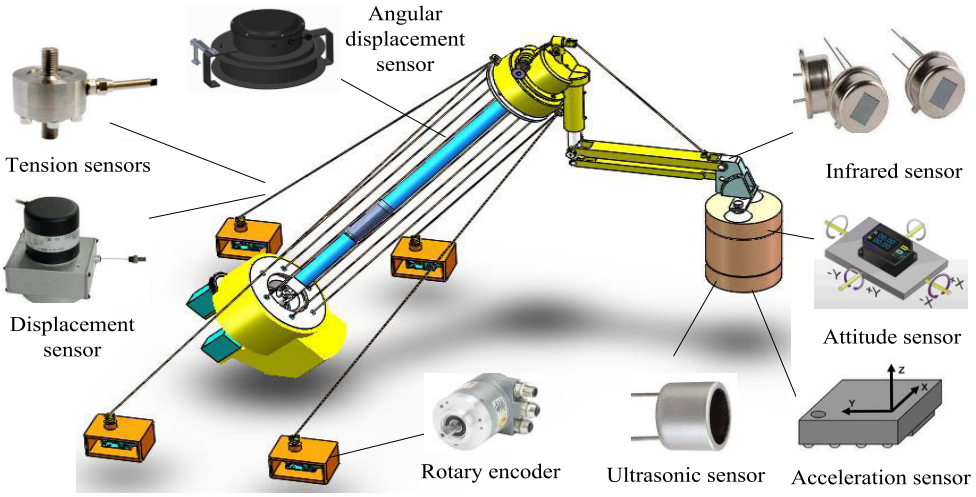

FIGURE 4. Assignment of the sensors.

TABLE 3. Sensors performance parameters.

	Angular	Displacement	Tension	Ultrasonic	Infrared	Attitude
Measuring range	0-360°	0-2000mm	0-100Kg	2-450cm	40cm	±4g
Output	0-20mA	4-24mA	700±5Ω	UART	100mA	Standard IIC
Nominal voltage	24V	24V	5-15V	5V	24V	5V
Accuracy	0.1%	0.05%	0.05%	3mm	1ms	±500°/s

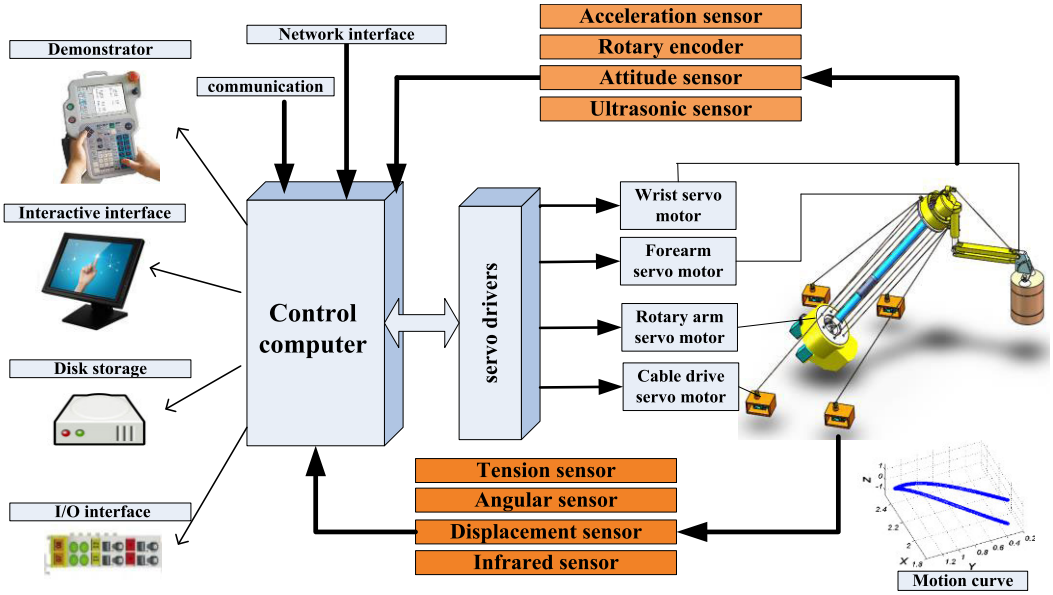

FIGURE 5. Control and measurement diagram of the CSPR.

where, θ_{ai} and θ_{qi} are the actual and expected angular displacements of the ith joint respectively.

Then, based on the angular displacement error and its derivative, the sliding mode surface function is constructed:

$$s(t) = \ddot{e} + \Lambda_1 \dot{e} + \Lambda_2 e \tag{22}$$

where, $\Lambda_i = diag(\lambda_{1i}, \lambda_{2i}, \cdots \lambda_{6i})$, and $\lambda_i > 0$

Finally, the sliding mode control law is designed as follows:

$$u = -\left(\frac{\Lambda_1 + \Lambda_2}{2}\right)^{-1} \left[{}^0J(\Theta)^T T_\tau + H - \eta \mathrm{sgn}(s)\right] \tag{23}$$

where, H is the error compensation term of modeling, and η is the sliding mode control parameter.

The simplified control principles for this control scheme are shown in Table 4.

V. NUMERICAL EXAMPLES

This section mainly analyzes the rationality and errors of the kinematics, dynamics and stiffness models of the CSPR through numerical examples. The basic parameters are shown in Table 5.

A. KINEMATIC SIMULATION

In order to verify the correctness of kinematics modeling analysis, the spatial position coordinates simulation analysis for the end-effector was been done with two working conditions of CSPR. Figure 6(a) shows the initial position of

TABLE 4. Simplified control principles.

1. **START** Initialization Detection
2. **Zero values:**(X_0, Y_0, Z_0). $\theta_{01}, \theta_{02}, \theta_{03}, \theta_{04}, \theta_{05}, \theta_{06}$
3. **INPUT** Target position or trajectory(X, Y, Z).
4. **Calculation:** $l_{A_iB_i}, l_{CD}, \theta_1, \theta_2, \theta_3, \theta_4, \theta_5, \theta_6, \tau$ ← **Kinematics and dynamics model**
5. **Joint movement:** Motor i Driver:
6. **Acquire:Sensor parameters:** Tension,Angular,Displacement
7. **Subtraction :** **errors** $\dot{e} = \dot{\theta}_{ai} - \dot{\theta}_{qi}, e = \theta_{ai} - \theta_{qi}$,
8. **If** $\dot{e} \le \zeta \quad e > \varepsilon_1$ then,

   intelligent controller: $\theta_{ai} = f(\theta_i, e)$

   Else if $\dot{e} > \zeta$

   Reduce operation speed

   Return to 4
9. **End if**

   Output $l_{A_iB_i}, l_{CD}, \theta_1, \theta_2, \theta_3, \theta_4, \theta_5, \theta_6$
10. **Display on the interface**

TABLE 5. Distance, angle parameter of the CSPR.

Distance(m)	a	b	c	d	e	f
	0.4	0.15	0.30	0.45	0.70	0.1
Angular angle(°)	θ_1	θ_2	θ_3	θ_4	θ_5	θ_6
	±42	±42	±180	±90	±90	±180

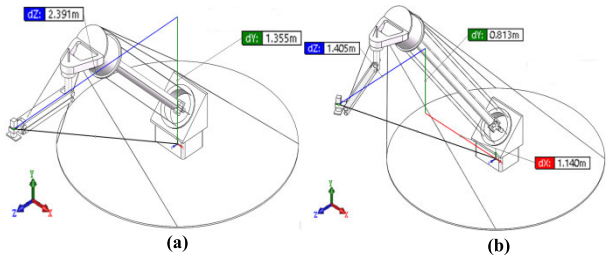

FIGURE 6. Exampled of forward kinematics with CSPR.

the robot ($\theta_i = 0$) and Figure 6(b) shows another position ($\theta_1 = 15, \theta_2 = 30, \theta_3 = 0, \theta_4 = -60, \theta_5 = -60, \theta_6 = -60$).

First, the position vector of the end-effector is obtained by the ''evaluation-measurement'' function. That is:

$$\begin{cases} p_{figa} = (Z_{figa}, Y_{figa}, X_{figa})^T = (2.391\ 1.3550)^T \\ p_{figb} = (Z_{figb}, Y_{figb}, , X_{figb})^T = (1.405\ 0.8131.140)^T \end{cases} \quad (24)$$

Then, angular angle of each joint was substituted into the kinematic model *Eq.*(5) and *Eq.*(6) respectively, and the the oretical value of the position vector of the end-effector under two working conditions could be obtained:

$$\begin{cases} p_{\exp a} = (p_{1a}, p_{2a}, p_{3a})^T = (2.3941.355\ 0)^T \\ p_{\exp b} = (p_{1b}, p_{2b}, , p_{3b})^T = (1.406\ 0.8121.141)^T \end{cases} \quad (25)$$

From *Eq.*(23) and Eq.(24), the position coordinate calculated by kinematics model is basically the same as the coordinate obtained by directly measured. The results can preliminarily verify that the kinematics analysis model is reasonable.

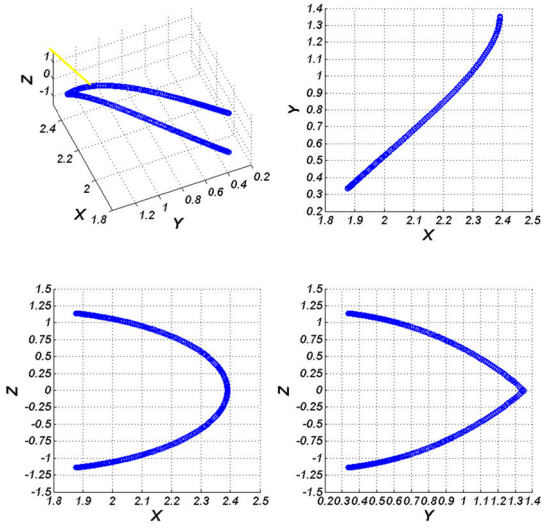

FIGURE 7. Motion trajectory of End-effector.

Then, to analyze the motion performance of the CSPR the dynamic motion simulation was carried out, and the motion equation of each joint of the CSPR is

$$\begin{cases} \theta_1(t) = (\pi/24) * (\cos(2*t) - 1) \\ \theta_2(t) = (-\pi/6) * \sin(t)\ ; \theta_3(t) = 0 * t \\ \theta_4(t) = \theta_6(t) = (\pi/3) * \sin(t) \\ \theta_5(t) = (-\pi/3) * |\sin(t)| \end{cases} \quad (26)$$

Based on the kinematics equation in section 3, the simulation got the motion trajectory of the end-effector shown in Figure 7.The first figure in Figure 7 represents the space motion trajectory of the end-effector, and the following three figures represent the projection of the motion trajectory toward the three basic planes.

Then, the length and velocity variation curve of the cables and the motion characteristic curve of the end-effector are obtained by simulation. The results are shown in Figure 8-15. Compared the desired parameters with the actual results, it can verify the correctness and the rationality of the dynamic analysis.

Figure 8 shows the expected angular displacement of each joint, and Figure 9 shows the actual angular displacement obtained in the simulation process. It can be seen that the actual angular displacement curve and the expected angular displacement curve have the same value and change trend, which verifies the correctness of the kinematic modeling.

Figure 10-11 shows the length variation curve of driven-cable B_iA_i and DC. It can be seen that the length of all driven-cable varies uniformly. There is a small fluctuation in the actual curve, but that will not affect the movement of the robot, which indicates that the design of structural parameters of the forearm and the rotating arm is reasonable

Figure 12 shows the desired trajectory of the end-effector. Compared desired trajectory with the actual motion curve

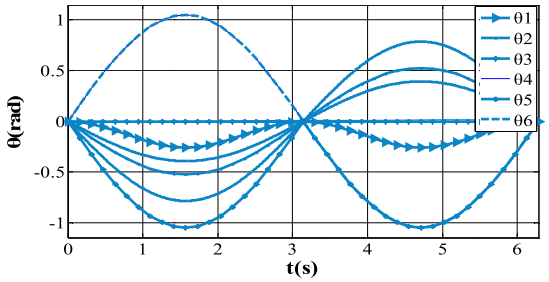

FIGURE 8. Desired angular displacement of joint.

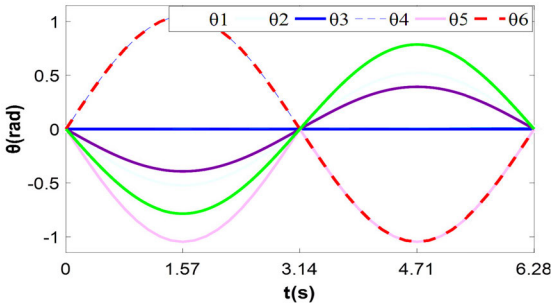

FIGURE 9. Actual angular displacement of joint.

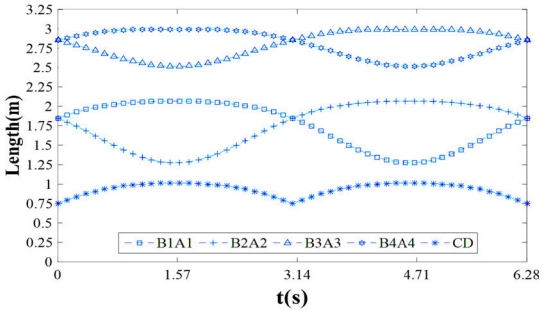

FIGURE 10. Desired length variation of driven-cable.

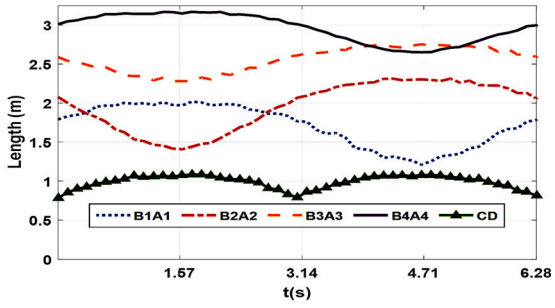

FIGURE 11. Actual length variation of driven-cable.

shown in Figure 13, it can be seen that the desired and actual trajectory curves are approximately the same, and the displacement coordinates in the *X*-*Y*-*Z* direction change almost exactly the same. The results can further show that the kinematics analysis of the CSPR is correct, and the kinetic characteristic of each joint have a good performance.

Figure 14 represent the velocity change of the four main driven-cable and the forearm driven cable. It shows that the

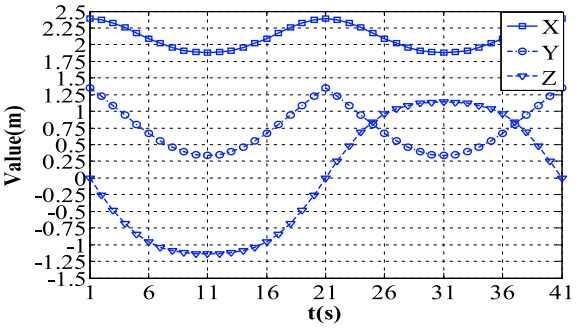

FIGURE 12. Desired motion trajectory of end-effector.

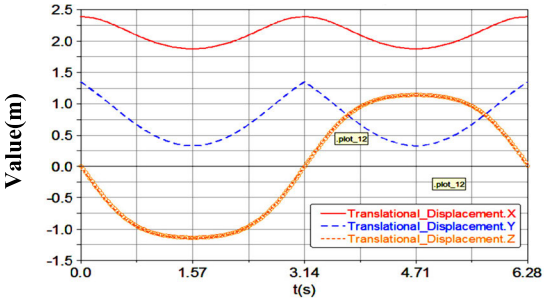

FIGURE 13. Actual motion trajectory of end-effector.

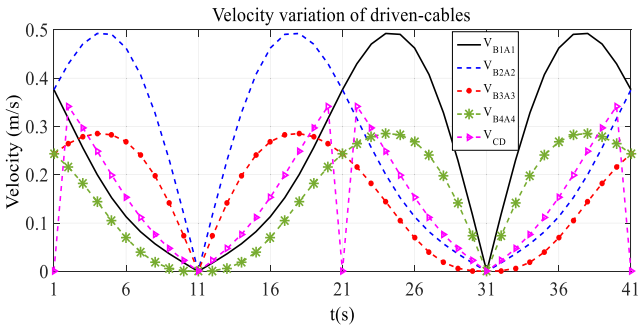

FIGURE 14. Driven-cable velocity in dynamics simulation.

motion law of each drive cable is basically consistent with the expected variation.

B. DYNAMICS SIMULATION AND ERROR ANALYSIS

In the following part, the parametric simulation of the robot will be carried out on the basis of the dynamic analysis in section 3. The velocity, acceleration and the errors are analyzed with considering the mass, gravity and inertia. The trajectory of the end effector is the same as that of the kinematics simulation. At the same time, The mass of the load captured by the end-effector is 20KG.

The simulation motion control strategy is sliding mode control method based on the position tracking parameters. According to *Eq.*(27), the control strategy parameters of the CSPR are designed as follows:

$$\begin{cases} \Lambda_1 = diag(50, 50 \cdots 50) \\ \Lambda_2 = diag(60, 60 \cdots 60) \\ \lambda = 3 \end{cases} \tag{27}$$

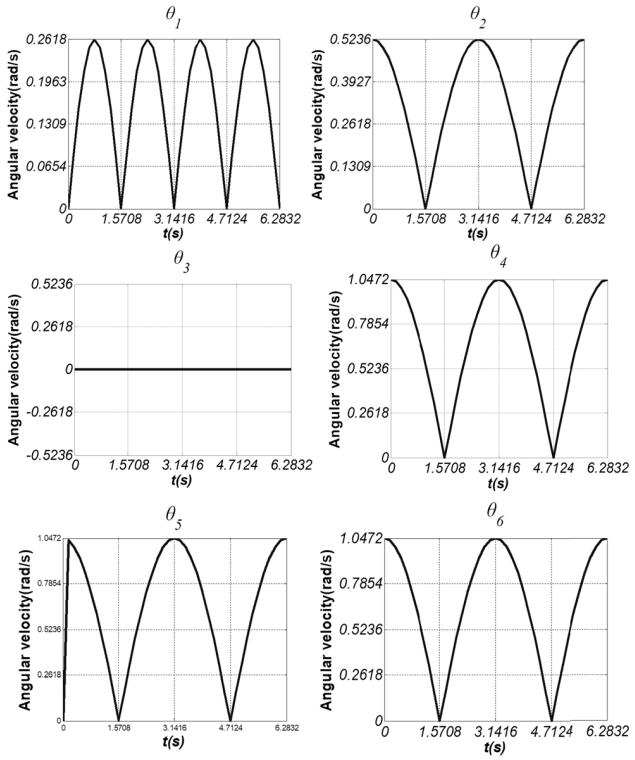

FIGURE 15. Expected angular velocity each joint.

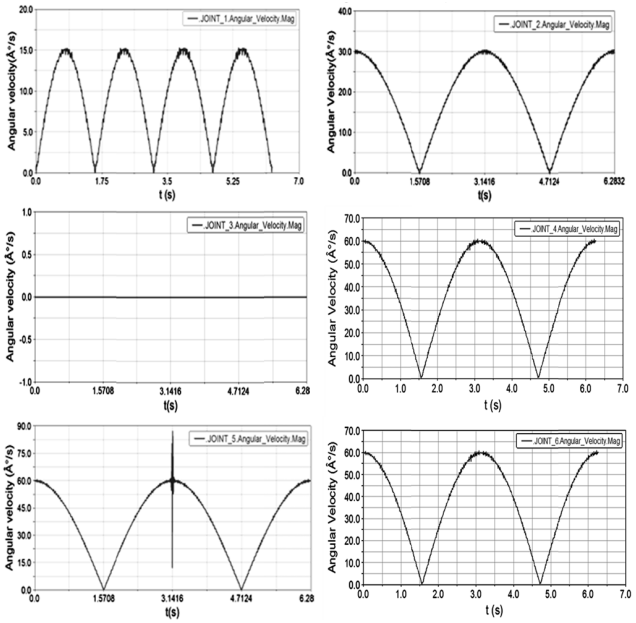

FIGURE 16. Actual angular velocity each joint.

Firstly, the angular velocity each joint are analyzed, and the simulation results are shown in Figure 15.

Figure 15-16 represents the angular velocity of each joint of CSPR during the dynamic simulation. It can be seen from the figures that the actual motion velocity curve of each joint and the expected curve are basically coincident, which indicates the correctness of the dynamic analysis. At the same time, the joint and the cable have a small range of vibration during the motion for the driving characteristics of universal joints, which will have an impact on the rapid working.

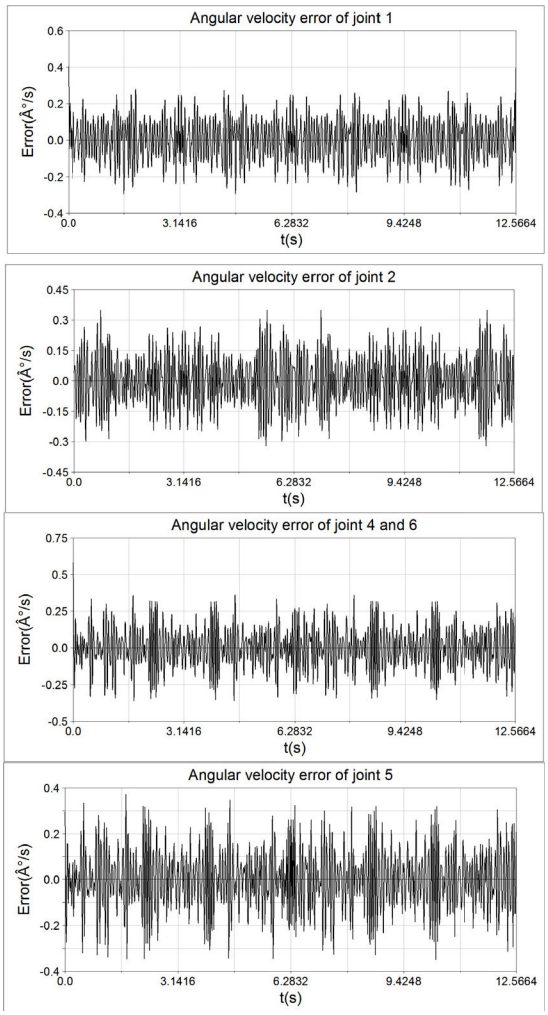

FIGURE 17. Angular velocity error with normal motion speed.

In order to analyze the magnitude of the velocity error, the motion error of the robot is analyzed at different speeds. The error deviation diagram is shown in Figures 17-18. Figure 17 shows the angular velocity error at a normal speed., and the error range is between ±0.2°/s. Compared to other joints, the angular velocity error of joint 1 is smaller than that of other joints.

Figure 18 shows the motion errors of each joint when the velocity is doubled. Compared to the error of normal velocity, the average speed error was within ±0.4°/s. Similarly, the angular velocity error of joint 1 is small, and there is a certain amplitude of fluctuation of joint 4 and 6. This errors are within the normal allowable range for handling work, which can guarantee the good motion performance of CSPR.

Figure 19 and 20 show the trajectory tracking and the motion errors of the end-effector in each direction. It can be seen that the end-effector can run smoothly along the desired trajectory, and the error in each direction is within a small range of 0.3mm.

C. RELIABILITY ANALYSIS OF CABLES

In the error analysis, the speed fluctuation and acceleration of the cable will cause the vibration of the driven-cables. It will

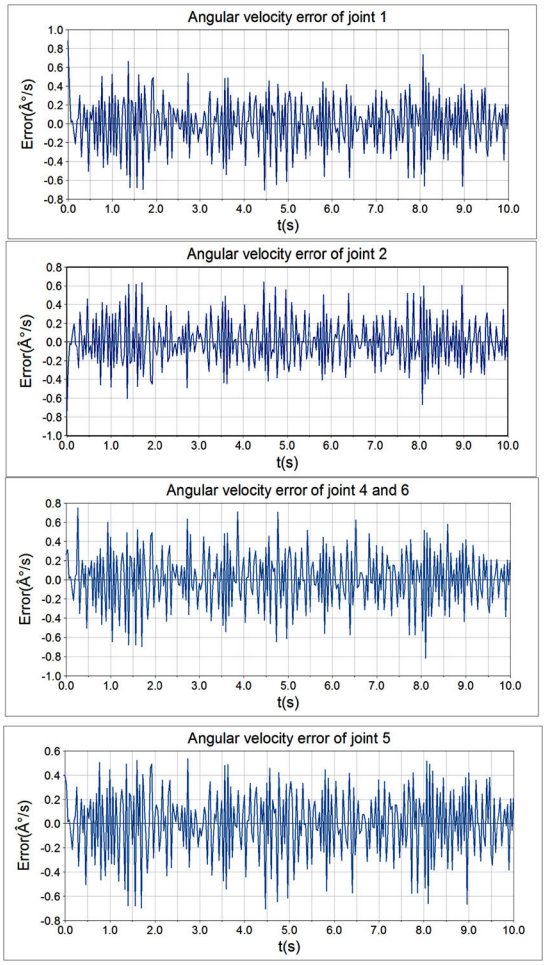

FIGURE 18. Angular velocity error with twice motion speed.

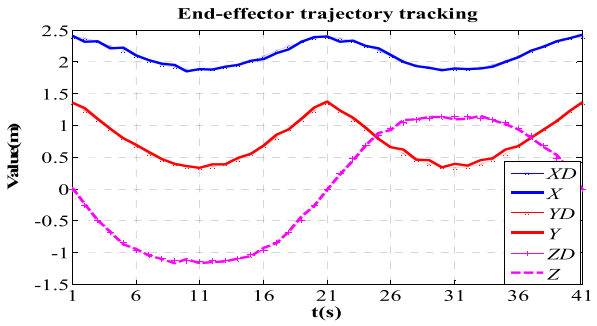

FIGURE 19. Trajectory tracking comparison.

cause the rope to jump out of the pulley groove when the vibration amplitude is large enough. In order to avoid this situation, The reliability analysis of cables will be analyzed in the following work based on the maximum jitter of each driven-cable.

The contact point of each driven-cable on its pulley is taken as the research object for this point is always the smallest stiffness point of the cables. At the same time, that is also the point with the largest vibration amplitude of the cable. In the simulation results, the velocity and acceleration curves of the smallest stiffness points on the driven-cables are shown in Figure 21.

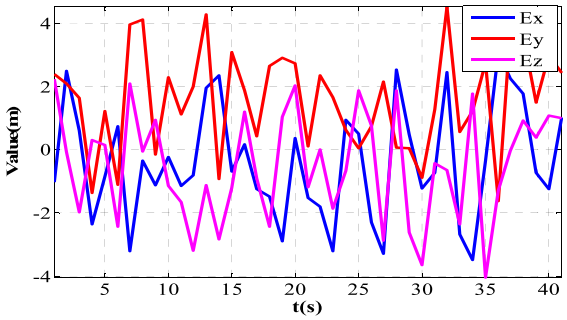

FIGURE 20. Trajectory error of End-effector.

TABLE 6. Maximum vibration amplitude and groove depth.

u_i ($10^{-3}m$)	u_1	u_2	u_3	u_4	u_5
	0.06	1.18	2.38	1.15	1.21
u_p ($10^{-3}m$)			20.00		

As shown in Figure 21, the dotted line represents the velocity of the smallest stiffness points, and the blue line represents the acceleration of the points. When the CSPR is working at normal speed, the mean velocity error amplitude of each joint is approximately distributed between 0.2 and 0.3 deg/s, and the other situation with twice speed is distributed between 0.4 and 0.5 deg/s, which will provide a basis for the definition of the rated working speed of the CSPR.

In order to analyze the reliability of the rope, we find the time position where the maximum acceleration is, and indicate them with the red arrow. Therefore, the maximum vibration amplitude of the cables can be expressed by the integral of the velocity within this time:

$$u_i = \int_0^{t_0} v(t)_i \mathrm{d}t \tag{28}$$

where, u_i is the vibration amplitude, $v(t)_i$ is the instantaneous velocity

The condition for the safe operation of the robot is "$u_i < u_p$", and u_p is the groove depth of guide sheave. The vibration amplitude of each cable can be calculated and the results are shown in Table 6.

According to the results in Table 6, the maximum vibration amplitude of the cables is 0.0615, 1.188, 1.152, 1.209(10^{-3}m), which are is far less than the groove depth of 20(10^{-3}m), and it can be clearly concluded that: $u_i < u_p$ The driven-cable would not jump out the pulley groove, and the working process is safe and reliable. In addition, the trend of the cable velocity curve in the Figure 21 is consistent with that in the Figure 15, which further verifies the correctness of the dynamics simulation of CSPR.

D. LOAD ANALYSIS

In order to further verify the safety and load carrying capacity of the CSPR under the different loading condition, this part will analyze the tensions of the driven-cables with load of 50Kg and 100Kg respectively. The working process of the manipulator with load is shown in Figure 22 [20].

Figure 22 shows the stacking process, and the motion trajectory of the end-effector is still the same as in the motion

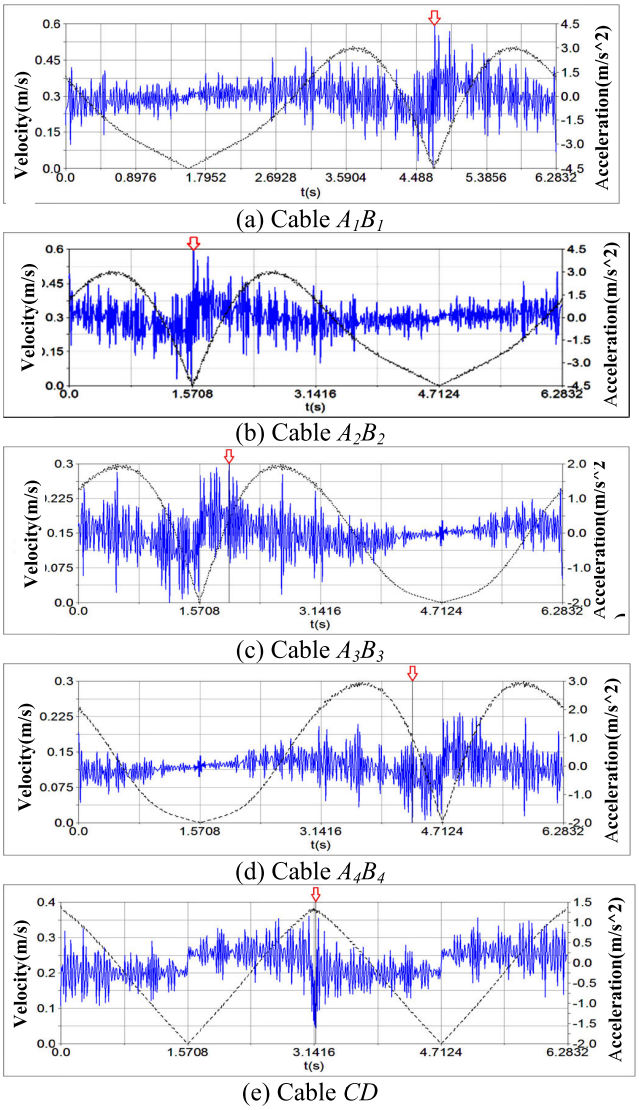

FIGURE 21. Velocity and acceleration curves of driven-cable.

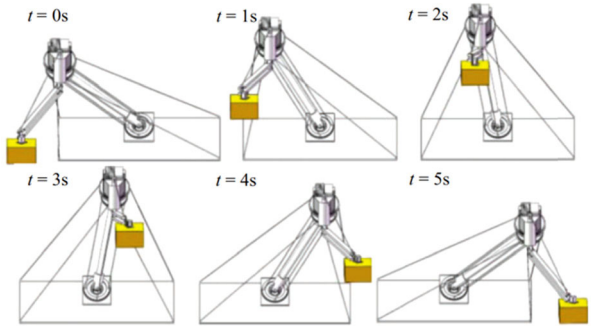

FIGURE 22. Stacking process with load.

simulation in part B. The motion of each joint is driven by four main actuated cables and one forearm actuated flexible, and the tensions for the five driven-cables of CSPR are shown in Figure 23.

As can be seen from Figure 23, cables 1 and 3 are installed behind the manipulator and subjected to greater tensions

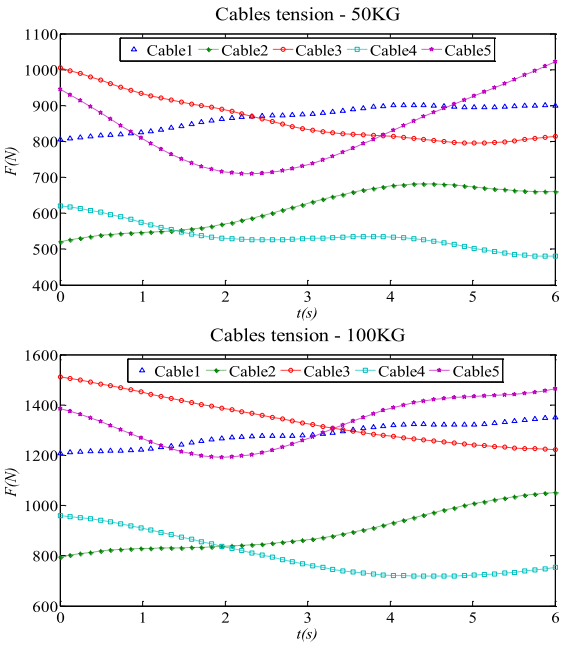

FIGURE 23. Tensions for the five driven-cables.

contrast with cables 2 and 4 located in the front part of the manipulator. On the other hand, the variation trend of the tensions of cables 1 and 4 are a gradually increased process, while the variation trend of cables 1 and 4 is on the contrary. Cable 5 is the driven-cable of the forearm, and the variation in tension is similar to the parabolic. In the simulation, the allowable tensions of the cables are 2200N with a diameter of 5mm. It can be get from Figure 23, the maximum tensions of the cables are all below 1600N no matter with load of 50kg or 100kg, which is completely less than the allowable tensions. So the working process is safe enough.

In conclusion, compared with the ordinary series rigid manipulator, the body mass of CSPR is only 30KG, however the maximum load reaches more than 100Kg. On the other hand, the operation error and accuracy are within the permissible range for stacking work, which further reflects the advantages of CSPR with light weight and large load.

VI. CONCLUSION

In this paper, the mechanical structure and transmission system of a cable-linkage serial-parallel palletizing robot is designed according to conventional series and parallel robots. Firstly, the DOF of the CSPR is calculated to determine the number of driven-cable. Then the forward and inverse kinematics equations of the CSPR are solved through homogeneous coordinate transformation method, and the dynamics model of the CSPR system is established with the Lagrangian method, so as to obtain the generalized force and torque acting on the end-effector and the joints. To improve motion accuracy and dynamic response performance, the closed-loop control system and control flow principle are designed based on a variety of sensors. Further, the dynamic simulation is carried out with the payload of 20Kg to verify the structural rationality, and the results show that the expected and

actual motion curves of each joint and the driven-cable are basically coincident. The driven-cables would not jump out the pulley groove. Finally, the tensions for the driven-cables of the CSPR are analyzed at loads of 50kg and 100kg, and the results have ensured the the safety and working performance of CSPR, which would provide theoretical basis for the development of cable-linkage serial-parallel palletizing robot.

REFERENCES

[1] C. Choubey and J. Ohri, "Optimal trajectory generation for a 6-DOF parallel manipulator using grey wolf optimization algorithm," *Robotica*, vol. 4, pp. 1–17, May 2020.

[2] Y. He, J. Mei, Z. Fang, F. Zhang, and Y. Zhao, "Minimum energy trajectory optimization for driving systems of palletizing robot joints," *Math. Problems Eng.*, vol. 2018, Dec. 2018, Art. no. 7247093.

[3] B. Hu, "Terminal position and orientation coupling in lower mobility robots," *J. Mech. Robot.*, vol. 11, no. 3, pp. 1–9, Jun. 2019.

[4] Y. Zhao, Y. Cao, C. Zhang, D. Zhang, and J. Zhang, "Error modeling and experimental study of a flexible joint 6-UPUR parallel six-axis force sensor," *Sensors*, vol. 17, no. 10, p. 2238, Sep. 2017.

[5] S. Qian, K. Bao, B. Zi, and N. Wang, "Kinematic calibration of a cable-driven parallel robot for 3D printing," *Sensors*, vol. 18, no. 9, p. 2898, Sep. 2018.

[6] M. A. Khosravi and H. D. Taghirad, "Dynamic modeling and control of parallel robots with elastic cables: Singular perturbation approach," *IEEE Trans. Robot.*, vol. 30, no. 3, pp. 694–704, Jun. 2014.

[7] C. Gosselin and S. Foucault, "Dynamic Point-to-Point trajectory planning of a two-DOF cable-suspended parallel robot," *IEEE Trans. Robot.*, vol. 30, no. 3, pp. 728–736, Jun. 2014.

[8] G. Abbasnejad, J. Eden, and D. Lau, "Generalized ray-based lattice generation and graph representation of wrench-closure workspace for arbitrary cable-driven robots," *IEEE Trans. Robot.*, vol. 35, no. 1, pp. 147–161, Feb. 2019.

[9] A. Aflakian, A. Safaryazdi, M. Tale Masouleh, and A. Kalhor, "Experimental study on the kinematic control of a cable suspended parallel robot for object tracking purpose," *Mechatronics*, vol. 50, pp. 160–176, Apr. 2018.

[10] G. Abbasnejad and M. Carricato, "Direct geometrico-static problem of underconstrained cable-driven parallel robots with five cables," *IEEE Trans. Robot.*, vol. 31, no. 2, pp. 468–478, Feb. 2017.

[11] Z. Gao and D. Zhang, "Performance analysis, mapping, and multiobjective optimization of a hybrid robotic machine tool," *IEEE Trans. Ind. Electron.*, vol. 62, no. 1, pp. 423–433, Jan. 2015.

[12] M. Gouttefarde, J.-F. Collard, N. Riehl, and C. Baradat, "Geometry selection of a redundantly actuated cable-suspended parallel robot," *IEEE Trans. Robot.*, vol. 31, no. 2, pp. 501–510, Apr. 2015.

[13] J.-P. Merlet, "Simulation of discrete-time controlled cable-driven parallel robots on a trajectory," *IEEE Trans. Robot.*, vol. 33, no. 3, pp. 675–688, Jun. 2017.

[14] N. Zhang, W. Shang, and S. Cong, "Geometry-based trajectory planning of a 3-3 cable-suspended parallel robot," *IEEE Trans. Robot.*, vol. 33, no. 2, pp. 484–491, Apr. 2017.

[15] K. Chadaj, P. Malczyk, and J. Fraczek, "A parallel recursive Hamiltonian algorithm for forward dynamics of serial kinematic chains," *IEEE Trans. Robot.*, vol. 33, no. 3, pp. 647–660, Jun. 2017.

[16] J. Hui, M. Pan, R. Zhao, L. Luo, and L. Wu, "The closed-form motion equation of redundant actuation parallel robot with joint friction: An application of the Udwadia–Kalaba approach," *Nonlinear Dyn.*, vol. 93, no. 2, pp. 689–703, Jul. 2018.

[17] X. Jiang, E. Barnett, and C. Gosselin, "Periodic trajectory planning beyond the static workspace for 6-DOF cable-suspended parallel robots," *IEEE Trans. Robot.*, vol. 34, no. 4, pp. 1128–1140, Aug. 2018.

[18] T. Sun, D. Liang, and Y. Song, "Singular-perturbation-based nonlinear hybrid control of redundant parallel robot," *IEEE Trans. Ind. Electron.*, vol. 65, no. 4, pp. 3326–3336, Apr. 2018.

[19] H. Wang, T. Gao, J. Kinugawa, and K. Kosuge, "Finding measurement configurations for accurate robot calibration: Validation with a cable-driven robot," *IEEE Trans. Robot.*, vol. 33, no. 5, pp. 1156–1169, Oct. 2017.

[20] B. Zi, B. Wang, and D. Wang, "Design and analysis of a novel cable-actuated palletizing robot," *Int. J. Adv. Robot. Syst.*, vol. 14, no. 6, Nov. 2017, Art. no. 172988141774108.

[21] Y. Tao, F. Chen, and H. Xiong, "Kinematics and workspace of a 4-DOF hybrid palletizing robot," *Adv. Mech. Eng.*, vol. 6, Jan. 2014, Art. no. 125973.

[22] M. Carricato, "Direct geometrico-static problem of underconstrained cable-driven parallel robots with three Cables1," *J. Mech. Robot.*, vol. 5, no. 3, Aug. 2013.

[23] J. Du and S. K. Agrawal, "Dynamic modeling of cable-driven parallel manipulators with distributed mass flexible cables," *J. Vib. Acoust.*, vol. 137, no. 2, pp. 1–8, Apr. 2015.

[24] B. Zi, Z. Zhu, and J. Du, "Analysis and control of the cable-supporting system including actuator dynamics," *Control Eng. Pract*, vol. 19, no. 5, pp. 491–501, Apr. 2011.

[25] J. Mo, Z.-F. Shao, L. Guan, F. Xie, and X. Tang, "Dynamic performance analysis of the x4 high-speed pick-and-place parallel robot," *Robot. Comput.-Integr. Manuf.*, vol. 46, pp. 48–57, Aug. 2017.

[26] W. He and Y. Dong, "Adaptive fuzzy neural network control for a constrained robot using impedance learning," *IEEE Trans. Neural Netw. Learn. Syst.*, vol. 29, no. 4, pp. 1174–1186, Apr. 2018.

[27] S. Roy and I. N. Kar, "Adaptive sliding mode control of a class of nonlinear systems with artificial delay," *J. Franklin Inst.*, vol. 354, no. 18, pp. 8156–8179, Dec. 2017.

[28] J. Guan, C.-M. Lin, G.-L. Ji, L.-W. Qian, and Y.-M. Zheng, "Robust adaptive tracking control for manipulators based on a TSK fuzzy cerebellar model articulation controller," *IEEE Access*, vol. 6, pp. 1670–1679, 2018.

[29] J. Xu, Q. Wang, and Q. Lin, "Parallel robot with fuzzy neural network sliding mode control," *Adv. Mech. Eng.*, vol. 10, no. 10, Oct. 2018, Art. no. 168781401880126.

[30] L. Angel and J. Viola, "Fractional order PID for tracking control of a parallel robotic manipulator type delta," *ISA Trans.*, vol. 79, pp. 172–188, Aug. 2018.

[31] B. Zi, G. Yin, and D. Zhang, "Design and optimization of a hybrid-driven waist rehabilitation robot," *Sensors*, vol. 16, no. 12, p. 2121, 2016.

[32] X. W. Kong and C. M. Gosselin, *Type Synthesis of Parallel Mechanisms*. Berlin, Germany: Springer-Verlag, 2007.

[33] P. Kuresangsai and M. O. T. Cole, "Kinematic modeling and design optimization of flexure-jointed planar mechanisms using polynomial bases for flexure curvature," *Mech. Mach. Theory*, vol. 132, pp. 80–97, Feb. 2019.

[34] A. Carpinteri, B. Chiaia, and P. Cornetti, "Static–kinematic duality and the principle of virtual work in the mechanics of fractal media," *Comput. Methods Appl. Mech. Eng.*, vol. 191, nos. 1–2, pp. 3–19, Nov. 2001.

[35] A. Elvin and J. Strydom, "Optimizing the design of tall buildings using the principle of virtual work: The effect of semi rigid connections," *Int. J. Steel Struct.*, vol. 6, pp. 1–21, Oct. 2020.

HUIHUI SUN was born in Xuzhou, Jiangsu, China, in 1989. He received the B.S. and M.S. degrees from the China University of Mining and Technology. He is currently a Lecturer with the North China Institute of Science and Technology. His research interests include the automatic motion control system of cable-driven parallel robot and series manipulator.

YUJIE ZHANG was born in Yingcheng, Hubei, China, in 1987. She received the B.S. and M.S. degrees from the Huazhong University of Science and Technology. She is currently a Lecturer with the North China Institute of Science and Technology. Since 2013, she has been the author of two books, five articles, and three patents. Her research interests include coal mine rescue robot and gait planning of quadruped robot.

BIN XIE was born in Hangzhou, Zhejiang, China. He received the M.S. degree from the School of Mechanical Engineering, Hefei University of Technology. Since 2015, he has been the author of two articles and three inventions. His research interests include series-parallel robot and palletizing robot.

BIN ZI received the Ph.D. degree in mechatronic engineering from Xidian University, Xi'an, China, in 2007. He is currently a Professor with the Hefei University of Technology, Hefei, China. He is the author of two books, more than 50 articles, and more than 30 inventions. His research interests include robotics and automation, mechatronics, and multirobot systems.